Chain-length-dependent intermolecular packing in polyphenylenes: a high pressure study

2003 J. Phys.: Condens. Matter 15 3375

(http://iopscience.iop.org/0953-8984/15/20/302)

INSTITUTE OF PHYSICS PUBLISHING JOURNAL OF PHYSICS: CONDENSED MATTER

J. Phys.: Condens. Matter **15** (2003) 3375–3389 PII: S0953-8984(03)57086-2

Chain-length-dependent intermolecular packing in polyphenylenes: a high pressure study

G Heimel[1], P Puschnig[2], M Oehzelt[1], K Hummer[2], B Koppelhuber-Bitschnau[3], F Porsch[4], C Ambrosch-Draxl[2] and R Resel[1]

[1] Institute of Solid State Physics, Graz University of Technology, Petersgasse 16, A-8010 Graz, Austria
[2] Institute for Theoretical Physics, University of Graz, Universitätsplatz 5, A-8010 Graz, Austria
[3] Institute of Physical and Theoretical Chemistry, Graz University of Technology, Technikerstrasse 4, A-8010 Graz, Austria
[4] Institute of Mineralogy and Petrology, University of Bonn, Poppelsdorfer Schloss, D-53115 Bonn, Germany

E-mail: georg.heimel@tugraz.at

Received 3 December 2002
Published 12 May 2003
Online at stacks.iop.org/JPhysCM/15/3375

Abstract

We report on pressure-induced structural changes in crystalline oligo(*para*-phenylenes) containing two to six phenyl rings. The results are discussed with particular emphasis put on the implications these changes in intermolecular distances and molecular arrangement have on important bulk properties of this class of materials, such as optical response and charge transport. We performed energy dispersive x-ray diffraction in a systematic study on polycrystalline powders of biphenyl, *para*-terphenyl, *p*-quaterphenyl, *p*-quinquephenyl and *p*-sexiphenyl under hydrostatic pressure up to 60 kbar. Revisiting the crystal structures at ambient conditions reveals details in the packing principle. A linear relationship between the density at ambient conditions and the number of phenyl rings is found. High pressure data not only yields pressure-dependent lattice parameters and hints towards pressure- induced changes in the molecular arrangement but also allows for an analysis of the equations of state of these substances as a function of oligomer length. We report the previously unknown bulk modulus of *p*-quaterphenyl, *p*-quinquephenyl and *p*-sexiphenyl ($B_0 = 83$, 93 and 100 kbar, respectively) and its pressure derivative ($B_0' = 6.4$, 7.5 and 5.6). A linear dependence of the bulk modulus on the inverse number of phenyl rings in the molecules and on their ambient conditions density is found.

1. Introduction

In the last three decades, since the discovery of conducting polyacetylene, π-conjugated hydrocarbon materials have attracted a lot of attention. In particular, π-conjugated organic

polymers seem to be promising candidates for low-cost, easy-processing materials for electro-optical and electronic applications. However, chemical and structural defects often make a quantitative understanding of the physical properties of these materials difficult. For that reason, shorter, crystalline, and thus ordered, oligomers of the parent polymers have been the focus of another, closely related line of research that has been successfully pursued for decades. The structural long range order in these (poly)crystalline, organic, π-conjugated molecules and their chemical purity not only make their intrinsic physical properties more easily accessible and understandable, but also permit their use in high performance device applications [1–3]. Approaches based on the self-assembly of smaller molecular units [4] or even polymers [5] now try to combine high purity and structural long range order with easier (solution) processability.

Significant insight into many properties of these materials can often be gained by studying a single, isolated molecule [6–8]. Nevertheless, for transport phenomena determining the performance of (opto)electronic devices, intermolecular interaction in terms of wavefunction overlap and low frequency (external) phonons will play a crucial role [9]. Moreover, important optical features such as the luminescence quantum yield in the solid state can drastically differ from that of the molecules in solution [10]. Last but not least, the strong anisotropy of the conductivity and the dielectric function often found in crystals of short polycyclic organic molecules [11] is closely related to the specific way of molecular packing. Hence, a detailed understanding of the crystal structure and the arrangement of the molecules relative to each other is a prerequisite for understanding important bulk and thin film properties in this class of materials.

In the present study we focus on the oligomers of poly(*para*-phenylene) (PPP), the oligo(*para*-phenylenes) (OPPs) containing two to six benzene repeat units: biphenyl (2P), *para*-terphenyl (P3P), *p*-quaterphenyl (P4P), *p*-quinquephenyl (P5P) and *p*-sexiphenyl (P6P). These molecules are representative of the group of rigid rod-like, polycyclic, π-conjugated compounds. While 2P can be seen as the simplest model system for this series of materials, P3P and P4P are used as UV laser dyes [12], in scintillation counters [13] and as wavelength shifters [14], whereas the longer P6P is used as the active layer in thin film organic LEDs (OLEDs) showing polarized blue emission [2]. Also the polymer PPP [15] and its planarized derivatives [16] have been extensively studied in optoelectronic applications.

A deeper insight into the nature of intermolecular interactions and the packing forces acting between molecules can be gained by modulating the intermolecular distances. Applying pressure to the sample is a 'clean' way to tune the degree of intermolecular interaction. A multitude of experiments have been conducted under high pressure on a variety of crystalline organic molecules yielding exciting results on structural [17], vibrational [18] and optical properties [19] as well as transport phenomena [20]. There are essentially two different kinds of atom–atom interactions in molecular crystals. On one hand there are strong, covalent intramolecular bonds and, on the other hand, there are weak, *van der Waals*-like forces acting between separate molecules. Since the former are stronger by at least two orders of magnitude than the latter (intermolecular phonons [21] at a few 10 cm^{-1}, intramolecular vibrons around [22] 1000 cm^{-1} and larger), it is justified to regard the molecules as *rigid bodies* upon compression as a first approximation.

2. Methodology

2.1. Experimental details

All measurements were performed at the beamline F3 at the HASYLAB of the DESY synchrotron facility in Hamburg, Germany. A detailed description of the beamline can be

found in [23]. For the experiments, that have been conducted in Debye–Scherrer geometry, we used white light radiation from a bending magnet. The scattered intensity was recorded with an energy dispersive Ge detector (∼10–60 keV) mounted at a fixed 2θ angle of about 2.5°. After the calibration of the energy scale with the Kα_1, Kα_2, Kβ_1 and Kβ_2 fluorescence lines of Ag, Eu, Te, Ta and Se, the detector angle was calibrated with Ag and NaCl as standards.

The OPP samples 2P and P4P have been purchased from Fluka, P3P from Aldrich and P6P from Tokyo Kasei Kogyo Co. Ltd. These chemicals were of >99% purity and were therefore used without further processing. P5P was synthesized following the Suzuki route [24] and purified by resublimation in a zone oven under an inert gas atmosphere.

In order to apply hydrostatic pressure, a Syassen–Holzapfel [25] type diamond anvil cell (DAC) with an Inconel gasket was used. As a pressure transmitting medium cryogenically loaded liquid nitrogen and a methanol:water 4:1 mixture was utilized. The pressure was determined by the ruby fluorescence method [26] and via the energetic position of the 111 and 200 reflections of NaCl and subsequently its equation of state (EOS) [27]. As could be concluded from the linewidth of the ruby fluorescence bands under pressure, hydrostaticity was guaranteed even when using no pressure transmitting medium at all. Two independent pressure runs were conducted for each of the materials.

2.2. Refinement

The Bragg peaks in energy dispersive x-ray diffraction (EDXD) patterns are rather broad and the energy resolution is low. Due to the resulting strong overlap between adjacent reflections and due to the very limited total number of observed peaks ($\leqslant$10), we could not hope to perform a Rietveld refinement on our data, which would have allowed us to extract additional structural information concerning the atomic positions within the unit cell. Instead, a LeBail fit [28] has been performed on the experimental diffraction patterns in order to determine the monoclinic unit cell parameters as a function of pressure. The fitted peak intensities and widths have not been further exploited. A Gaussian lineshape has been assumed for the diffraction peaks of the sample and the NaCl pressure calibrant. While the total fit is relatively stable concerning the a and b lattice constants, c and β are harder to determine independently, since the $00l$ reflections only yield the unit cell height $c \sin\beta$. Pairs of reflections with indices hkl and $-hkl$ are needed to separate c and β:

$$d_{hkl} = \frac{\sin\beta}{\sqrt{\left(\frac{h}{a}\right)^2 + \left(\frac{k}{b}\right)^2 \sin^2\beta + \left(\frac{l}{c}\right)^2 + \frac{2hl}{ac}\cos\beta}}. \tag{1}$$

In addition to that, an error on c (being the longest lattice constant) contributes least to the total error of the fit, as can be seen from equation (1) (c in denominator). Consequently, the scattering and the error on c and β is higher than on a and b.

3. Results and discussion

3.1. Crystal structures at ambient conditions

At room temperature the OPP molecules all crystallize in the monoclinic space group $P2_1/a$ with $Z = 2$ molecules per unit cell. These two translationally inequivalent molecules sit at 000 and $\frac{1}{2}\frac{1}{2}0$. The molecules are arranged in layers parallel to the ab plane with the long molecular axes almost perpendicular to the plane of the layer. The molecules within such a layer are arranged in the so-called *herringbone*-pattern. Figure 1 shows a view along the long axes of the molecules of one layer. The distinctive pattern is determined by the unit cell axis a and b

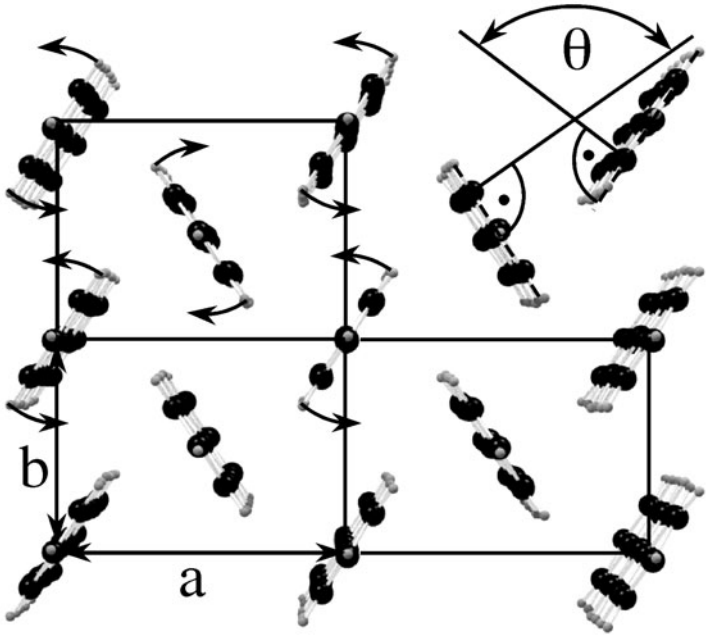

Figure 1. View along the long axes of molecules within one layer of a *para*-terphenyl crystal. The herringbone angle θ is defined as the angle between the planes of two translationally inequivalent molecules. The two shorter lattice constants a and b determine the rectangle that is the base plane of the unit cell. Upon applying hydrostatic pressure, the unit cell axis a shortens twice as much as the unit cell axis b and the molecules twist around their long axis as indicated by the curved arrows. For more details refer to the text.

and the herringbone angle θ, the angle between the planes of two translationally inequivalent molecules. In figure 2 we represent the arrangement of two layers of molecules relative to each other. The long molecular axes come to lie within the *ac* plane and are tilted with respect to the c^* axis (perpendicular to the *ab* plane) by the setting angle χ. While the unit cell height h ($=c \sin \beta$) determines the interlayer distance, the monoclinic angle β determines the way two layers are packed on top of each other. Note that χ not only determines the specific topology of the top and bottom 'surfaces' of one such layer but also describes a kind of 'linear slip' s (see figure 2) between two adjacent molecules within one layer. Aromatic rings tend not to stack directly in a coplanar way. One always observes a tilt and a slip between molecules in polyaromatic compounds [29]. In table 1 we report the literature data [30–35] on the unit cell parameters a, b, c and β, the molecular arrangement determined by θ and χ as well as the unit cell volumes V_0 and the densities ρ_0 of the investigated substances at ambient pressure and room temperature.

While the unit cell axes a are practically equal for oligomers of any length (as is b), c, h and V_0 increase linearly with increasing oligomer length n. The setting angle χ is approximately equal for all oligomer lengths as a result of the intermolecular packing forces within one layer. Consequently, the monoclinic angle β does not evolve monotonically with the number of rings in the molecule, because it needs to readjust the layers on top of each other in order to provide a comparable interlayer stacking for all compounds. Additionally, the unit cell of the shortest and the longest molecule, 2P and P6P, is chosen a little different from that of the oligomers P3P, P4P and P5P. In contrast to 2P and P6P, where the c axis is tilted (with respect to the c^*

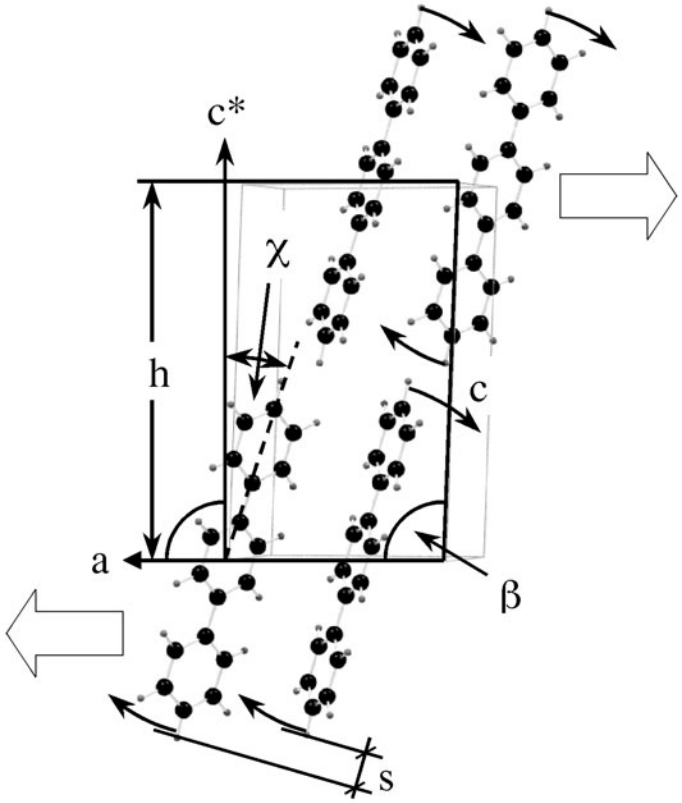

Figure 2. Side view of the unit cell of *para*-terphenyl. The molecules form layers with the molecular axis tilted by the *setting angle* χ with respect to c^* (perpendicular to the *ab* plane). This brings the molecules out of a totally coparallel arrangement by inducing a 'linear slip' s between adjacent molecules along the a direction. The monoclinic angle β is responsible for the way two layers adjust on top of each other. It also relates the unit cell height h to the lattice parameter c. Upon applying hydrostatic pressure the molecules tilt, as indicated by the curved arrows, and the two layers slide in the directions indicated by the broad arrows. For more details see the text.

axis) in the direction opposite to the long molecular axis, in P3P, P4P and P5P (see figure 3(a)), the c axis and the long molecular axis are tilted in the same direction with respect to the c^* axis (see figure 3(b)). The molecular arrangement is similar; only the unit cell choice is different in a way that $+a$ in 2P and P6P corresponds to $-a$ in P3P, P4P and P6P.

At this point we would like to revisit in more detail the data listed in table 1. A closer inspection reveals that the unit cell volume at ambient pressure V_0 increases linearly with oligomer length n, with a slope $k_{V_0} = 64.19$ Å^3 and an axis intercept of $d_{V_0} = 184.56$ Å^3. Since also the molecular (and unit cell) mass m increases linearly with n (slope $k_m = 152$ amu, axis intercept $d_m = 4$ amu), we can derive the analytic chain length dependence of the ambient pressure density ρ_0 as

$$\rho_0 = \frac{k_m n + d_m}{k_{V_0} n + d_{V_0}} \approx k_{\rho_0} \frac{1}{n} + d_{\rho_0}. \tag{2}$$

As indicated in equation (2), one can develop the centre expression into a Taylor series over the inverse number of phenyl rings $(1/n)$ up to first order to get an (approximate) linear relationship between ρ_0 and $1/n$ on the far right-hand side. Developing around the centre $1/n = 1/3$ of

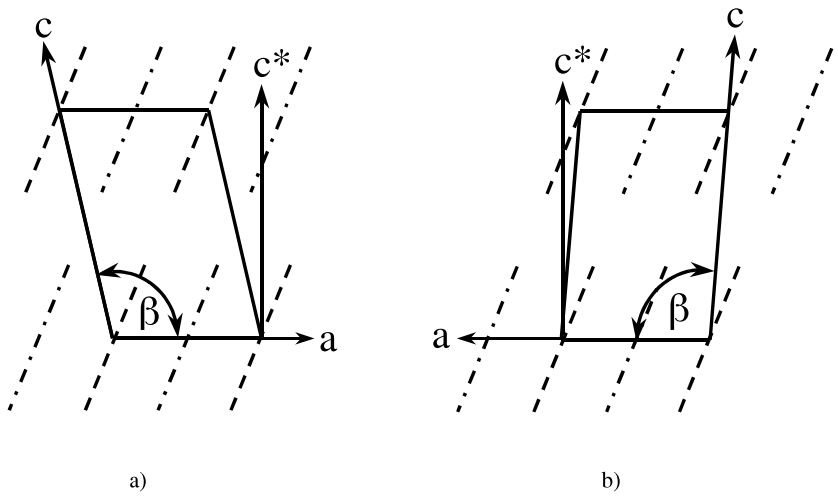

Figure 3. Schematic representation of the two different unit cell choices for oligo(*para*-phenylenes). In the unit cell of biphenyl and *p*-sexiphenyl (a), the *c* axis is tilted in the opposite direction with respect to the c^* axis as the molecules are tilted, while for *p*-terphenyl, *p*-quaterphenyl and *p*-quinquephenyl (b) the *c* axis and the molecules are tilted in the same direction. The broken and chain lines represent the two different groups of translationally inequivalent molecules. See the text for details.

Table 1. Monoclinic lattice parameters a, b, c and β of the oligo(*para*-phenylenes) biphenyl (2P), *p*-terphenyl (P3P), *p*-quaterphenyl (P4P), *p*-quinquephenyl (P5P) and *p*-sexiphenyl (P6P) together with the herringbone angle θ and the setting angle χ that determine the orientation of the two inequivalent molecules relative to each other and to the unit cell edges. Also reported are the respective unit cell height h ($=c \sin\beta$), the unit cell volume V_0 and the densities ρ_0 at ambient pressure and room temperature.

Material	a (Å)	b (Å)	c (Å)	β (deg)	h (Å)	V_0 (Å^3)	θ (deg)	χ (deg)	ρ_0 (amu Å^{-3})
2P[a]	8.12	5.64	9.47	95.40	9.43	431.77	113.76	17.37	0.713
2P[b]	8.12	5.63	9.51	95.10	9.47	433.03	112.50	17.09	0.711
P3P[c]	8.11	5.61	13.61	92.02	13.60	618.99	114.13	17.47	0.743
P3P[d]	8.08	5.60	13.59	91.92	13.58	614.58	—	—	0.748
P4P[e]	8.11	5.61	17.91	95.80	17.82	810.68	114.13	17.47	0.755
P5P[f]	8.07	5.58	22.06	97.91	21.85	983.92	114.38	17.40	0.776
P6P[f]	8.09	5.57	26.24	98.17	25.97	1170.18	114.45	17.60	0.783

[a] Values taken from [30].
[b] Values taken from [31].
[c] Values taken from [32].
[d] Values taken from [33].
[e] Values taken from [34].
[f] Values taken from [35].

our interval of interest (1/2 to 1/6) yields a $k_{\rho_0} = -0.21$ amu Å^{-3} and $d_{\rho_0} = 0.82$ amu Å^{-3}. This analytical chain length dependence of the ambient pressure density ρ_0 of the OPPs is shown in figure 4 together with the literature data from table 1.

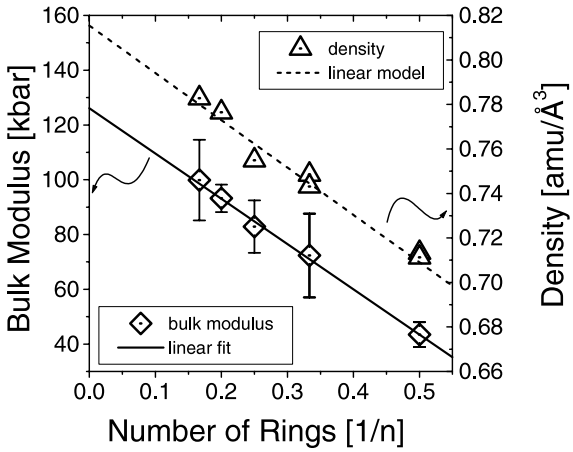

Figure 4. Bulk modulus of the oligo(*para*-phenylenes) containing two (2P) to six (P6P) phenyl rings as a function of the inverse number of phenyl rings $1/n$. The error bars indicate the statistical errors of the fit of the Murnaghan EOS (equation (3)) to our experimental data (see figure 8). The full line is a linear regression on our experimental data. The triangles refer to the right-hand side y axis and represent the densities of the oligo(*para*-phenylenes) as a function of the inverse number of phenyl rings $1/n$ (see table 1). The broken line through the density points represents our model chain length dependence (see equation (2) and the text for details).

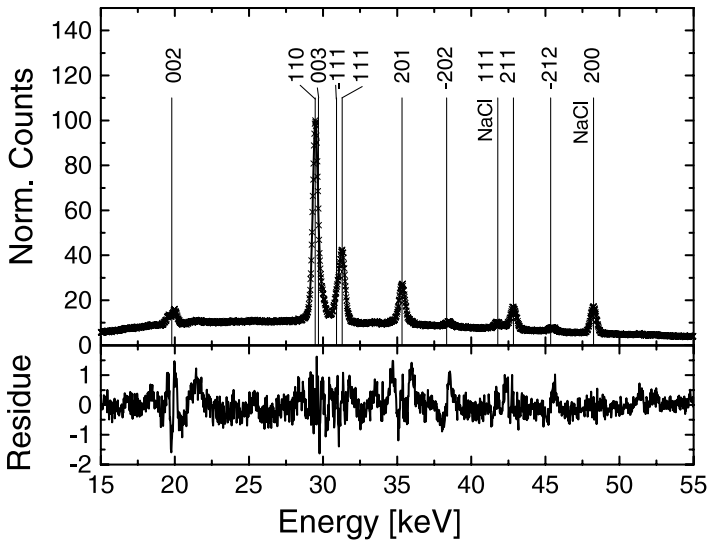

Figure 5. EDXD pattern of *p*-terphenyl recorded at ∼2 kbar. The crosses in the upper panel correspond to the experimental data, while the full line represents our fit. The lower panel shows the residue. The thin vertical lines mark the position of those reflections for which Miller indices are given above them. Note that the two lines at ∼42 and ∼48 keV are the *111* and *200* reflections of the NaCl pressure calibrant.

3.2. Chain-length-dependent compressibilities

In order to give an impression of the quality of the diffraction patterns and our peak fitting procedure, we present in figure 5 a sample diffraction pattern of P3P at ∼2 kbar together

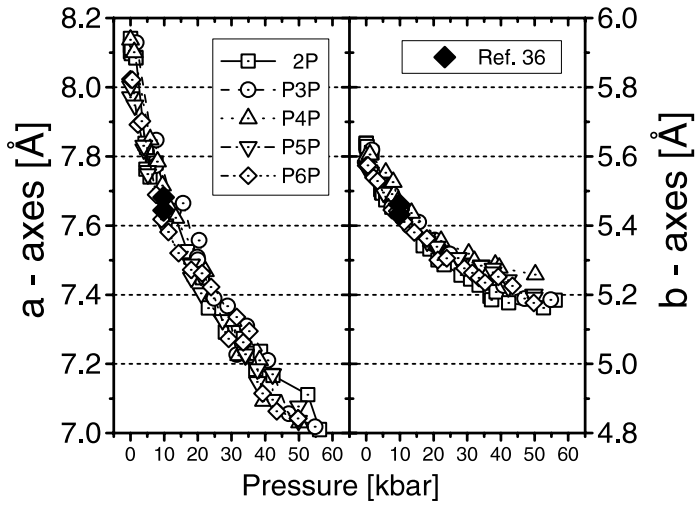

Figure 6. Lattice parameters a (left panel) and b (right panel) of oligo(*para*-phenylenes) containing two to six phenyl rings as a function of hydrostatic pressure. The left and right y axis cover the same range (1.2 Å). The lattice parameters of all oligomers have the same length at ambient conditions and moreover show the same pressure dependence. Note that lattice constant a is reduced approximately twice as much as lattice constant b in this pressure region. The filled symbols are data taken from [36].

with the Miller indices of the respective Bragg peaks. The pattern has been normalized to 100 counts. The crosses in the upper panel represent the experimental data, the full line corresponds to our fit and in the lower panel the difference between the experimental and fitted pattern is shown.

From these refinements, we were able to determine the monoclinic lattice parameters of 2P, P3P, P4P, P5P and P6P up to about 60 kbar. At pressures higher than that, the decreasing signal to noise ratio prohibits recording diffraction patterns within a reasonable integration time. In figure 6, the lattice constants a and b are plotted against pressure p. One can see that not only are the values at ambient pressure virtually identical (see table 1) but so also is their pressure dependence. The left and right y axes in figure 6 span the same length (1.2 Å). While a decreases by around $\Delta a \approx -1.1$ Å up to ∼60 kbar ($\Delta a/a \approx -14\%$), b decreases less than half of the amount of a ($\Delta b \approx -0.4$ Å, $\Delta b/b \approx -7\%$). These findings agree well with previously published results available [36] for 2P and P3P (see figure 6).

In figure 7, we present the monoclinic angle β, the lattice constant c and the unit cell height h as a function of pressure for 2P to P6P. The values for c and h at ambient pressure (c_0 and h_0, respectively) have been subtracted for better comparison between different oligomer lengths. As one would expect, the layer thickness h decreases for all molecules (about -0.6 Å for 2P to P5P and around -1.0 Å for P6P). Also, the lattice constant c decreases with pressure (∼-0.4 to ∼-1.2 Å). Interestingly, the monoclinic angle β decreases for 2P and P6P (by about $-4°$) while it increases for P3P, P4P and P5P by roughly the same amount. This will be discussed in more detail below.

In order to extract the bulk moduli of the investigated compounds we fit Birch [37], Murnaghan [38] and Vinet [39] EOS to the unit cell volume V ($=abc\sin\beta$) as a function of pressure. These three types of EOS yielded slightly different results. Literature data on the unit cell volume change with pressure exist for 2P and P3P up to 35–45 kbar although no concise information can be found on the effect of pressure on the lattice parameters [36, 40, 41]. The

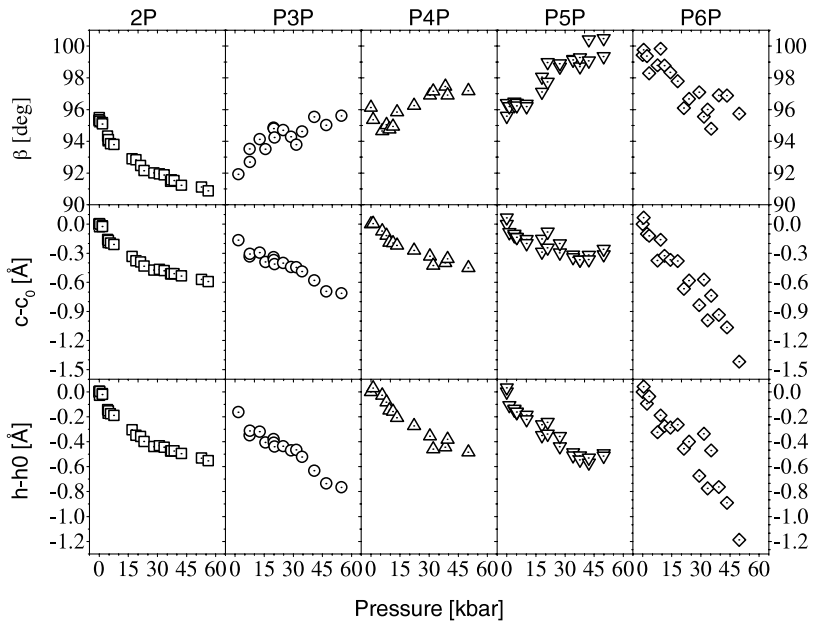

Figure 7. Monoclinic angle of the oligo(*para*-phenylenes) biphenyl (2P, outermost left top panel) to *p*-sexiphenyl (P6P, outermost right top panel) as a function of hydrostatic pressure. The middle panels show the pressure-induced decrease of the lattice constant c and the lower panels show that of the unit cell height h. For the sake of clarity the ambient pressure values for c and h (c_0 and h_0 from table 1) have been subtracted.

Murnaghan EOS has been used on 2P and P3P before [41]. Performing a least squares fit of Murnaghan's EOS in its form $V = f(p)$ (see equation (3)) to all of these literature data yields a chi-squared value at least four orders of magnitude smaller than with any other EOS. Hence, we conclude that this EOS is best suited to describe OPPs in that pressure range (and to compare our findings with literature data). The analytical form of the Murnaghan EOS we used is

$$V = V_0\left(1 + \frac{B_0' p}{B_0}\right)^{\frac{-1}{B_0'}} \tag{3}$$

where B_0 is the bulk modulus and B_0' is its derivative with pressure. In figure 8 the unit cell volumes are plotted as a function of pressure together with the best fits according to equation (3). The numerical values for V_0, B_0 and B_0' are given in table 2 together with the above-mentioned previous results on 2P and P3P. One has to keep in mind that our data can only be compared to the literature if one restricts the fit to the (lower) maximum pressures achieved therein. In the topmost block of table 2, we list our results up to 60 kbar. The values presented in the middle block of table 2 are obtained by fitting either the $V(p)$ or the $V/V_0(p)$ data found in the literature to our EOS (equation (3)), where the numbers in brackets result from fitting our data up to the same maximum pressure as reached in the experiments they are compared to (35 kbar in [36], 40 kbar in [40] and 45 kbar in [41]). In the lower block of table 2 the values for B_0 and B_0', as determined by Vaidya and Kennedy [41] (who use a slightly modified EOS on their own data set as well as on that of Bridgman [42]), are given.

In figure 4 the values for B_0 from table 2 and ρ_0 from table 1 are plotted against the inverse number of phenyl rings n. We note the linear dependence of both B_0 and ρ_0 as a function of

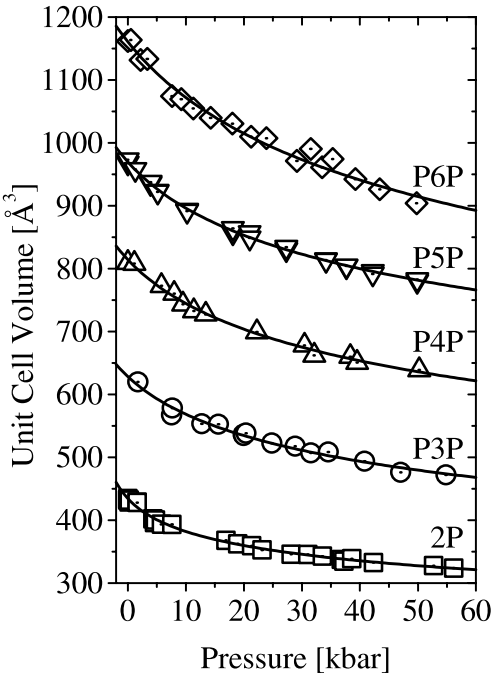

Figure 8. Unit cell volume of oligo(*para*-phenylenes) containing two (2P) to six (P6P) phenyl rings (from bottom to top) as a function of hydrostatic pressure. The symbols represent the experimental data while the full curves are the least squares fits to the Murnaghan EOS (equation (3)).

$1/n$ (see also equation (2)). Higher density means less compressible volume 'between' the molecules and thus a higher bulk modulus (a lower compressibility). As a consequence of the data presented in figure 4 and the brief discussion above (equation (2)), one can expect a linear dependence of B_0 on ρ_0, which is indeed found (see figure 9).

3.3. Rearrangement of the molecules

We would now like to address the question of the arrangement of the molecules in the unit cell and relative to each other. As one can learn from figure 7, the unit cell height h decreases upon increasing pressure for all oligomer lengths. Looking at the molecular layer arrangement in figures 2 and 3 leads to the conclusion that the molecules can only give way by tilting more strongly with respect to the c^* axis, thus increasing χ. As a consequence, the monoclinic angle β must increase in P3P, P4P and P5P and decrease in 2P and P6P in order to conserve the interlayer stacking, e.g. the way in which the top and bottom 'surfaces' of two adjacent layers come to lie with respect to each other regarding the displacement in the a direction. In figure 7 one can see that this expected behaviour of β corresponds to the outcome of the experiments. In 2P and P6P, the top layer slips in the a direction, while it slips in the $-a$ direction in the case of P3P, P4P and P5P in order to readjust the position of two layers relative to each other. The above discussed mechanism of pressure-induced molecular rearrangement is schematically depicted in figure 2 for the sample case of P3P. Note that increasing χ means also an increased linear slip s (see figure 2) of two adjacent molecules within one layer along the a direction and thus an increasing deviation from the strictly coparallel arrangement of said molecules. Assuming the unit cell height h to be equal to the 'height' one molecule needs

Table 2. In the uppermost block we report the unit cell volume at ambient pressure V_0, the bulk modulus B_0 and its pressure derivative B_0' of biphenyl (2P), *p*-terphenyl (P3P), *p*-quaterphenyl (P4P), *p*-quinquephenyl (P5P) and *p*-sexiphenyl (P6P). All parameters were determined by fitting the Murnaghan EOS (see equation (3)) to our experimentally determined pressure-dependent unit cell volume V. In the two lower blocks we list the results found in the literature for 2P and P3P. The values in brackets in the two lower blocks are obtained by fitting our data to the Murnaghan EOS (see equation (3)) up to the same maximum pressure as reached in the experiment they are compared to.

	Material	V_0 (Å^3)	B_0 (kbar)	B_0'
Our data up to 60 kbar	2P	434.28	43	8.4
	P3P	628.30	72	6.1
	P4P	814.18	83	6.4
	P5P	969.65	93	7.5
	P6P	1160.66	100	5.6
Literature V/V_0 data fitted to our EOS	2P[a]	433.16[d]	59(45)	12.9(8.1)
	2P[b]	—	50(48)	8.6(7.9)
	2P[c]	—	51(48)	8.2(7.9)
	2P[c]	—	52(48)	8.2(7.9)
	P3P[a]	615.05[d]	57(44)	12.7(7.7)
	P3P[b]	—	67(65)	8.3(8.3)
	P3P[c]	—	58(65)	8.4(8.3)
B_0 and B_0' as reported in [41]	2P[c]	—	54(48)	7.8(7.9)
	2P[c]	—	45(48)	9.9(7.9)
	2P[c]	—	54(48)	7.9(7.9)
	2P[c]	—	51(48)	8.6(7.9)
	P3P[c]	—	60(65)	8.1(8.3)
	P3P[c]	—	54(65)	8.1(8.3)

[a] Values taken from [36] (data up to 35 kbar).
[b] Values taken from [40] (data up to 40 kbar).
[c] Values taken from [41] (data up to 45 kbar).
[d] Since $V(p)$ instead of just $V/V_0(p)$ is given in [36], V_0 could also be extracted from the fit.

in the crystal and neglecting compression of the interlayer distance permits us to estimate this pressure-induced increase of χ. From the respective values at ambient pressure, h_0 and χ_0 one can easily calculate the *effective length* l of a molecule as

$$l = \frac{h_0}{\cos \chi_0}. \tag{4}$$

Provided l does not change with pressure (rigid body) we can further estimate χ at any pressure p as

$$\chi = \arccos\left(\frac{h(p)}{l}\right). \tag{5}$$

The estimated values for $\Delta\chi$ $(=\chi_0 - \chi)$ up to maximum pressure are summarized in table 3. They compare reasonably well to *ab initio* results on 2P [43] and P3P [44] and to experimental results found for similar compounds [45].

Considering the molecular arrangement within the herringbone pattern depicted in figure 1 and the fact that not only the absolute but also the relative decrease of the lattice constants a is more than twice that of the lattice constants b (see figure 6) leads to the only plausible conclusion of how the molecules can react to the external stress. The molecular arrangement must relax by increasing the herringbone angle θ (see figure 1 and table 1). This mechanism is schematically represented in figure 1, where the molecules located at 000 turn counterclockwise and those

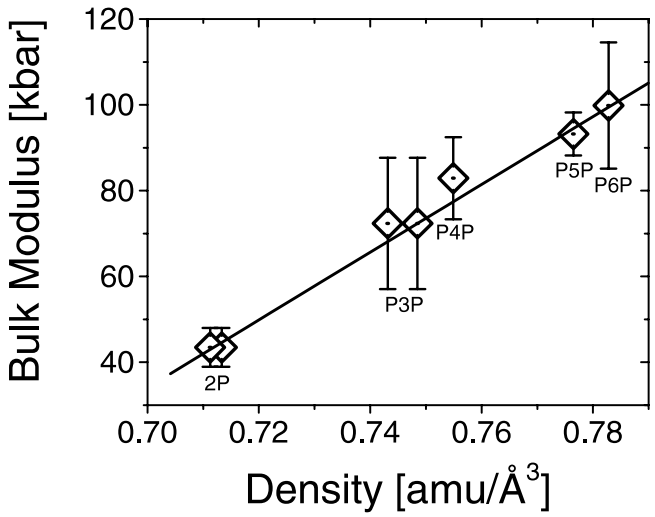

Figure 9. Bulk modulus of the oligo(*para*-phenylenes) containing two (2P) to six (P6P) phenyl rings versus their respective density (see table 1). The error bars are the statistical errors of the fit of the Murnaghan EOS (equation (3)) to our experimental data (see figure 8). The full line is a linear regression of our experimental data.

Table 3. Estimate of the pressure-induced increase of the setting angle χ between long molecular axis and the c^* axis. The unit cell height at ambient pressure h_0 and its value at 60 kbar $h_{60\ \mathrm{kbar}}$ were taken from figure 6. The setting angle at ambient pressure χ_0 was taken from table 1. The effective molecular length l and the setting angle at 60 kbar $\chi_{60\ \mathrm{kbar}}$ were calculated according to equations (4) and (5), respectively. The change of χ from ambient pressure to 60 kbar $\Delta\chi_{\max} = \chi_{60\ \mathrm{kbar}} - \chi_0$ is also listed.

Material	h_0 (Å)	χ_0 (deg)	l (Å)	$h_{60\ \mathrm{kbar}}$ (Å)	$\chi_{60\ \mathrm{kbar}}$ (deg)	$\Delta\chi_{\max}$ (deg)
2P	9.45	17.23	9.89	8.90	25.90	8.67
P3P	13.55	17.47	14.20	12.95	24.23	6.81
P4P	17.80	17.47	18.66	17.25	22.42	4.95
P5P	21.80	17.40	22.85	21.20	21.88	4.48
P6P	26.00	17.60	27.28	24.80	24.61	7.01

located at $\frac{1}{2}\frac{1}{2}0$ rotate clockwise around their long axis, thus approaching a cofacial, brick-like arrangement. Contrariwise, a higher compressibility along the *a* axis than along the *b* axis can be motivated by the fact that the translationally equivalent molecules are more closely packed in the latter direction compared to the former. Additionally, the pressure-induced rotation of the molecules along their long axis (increase of the herringbone angle θ) can only be caused by the interaction of translationally non-equivalent molecules. Again, these considerations are in accordance with previously found results on comparable compounds [43–45].

3.4. Outreach

Clearly, a smaller unit cell leads to an increased overlap between the electronic wavefunctions of the individual molecules, especially between those within one layer (parallel to the *ab* plane). This increase in electronic interaction will have several consequences regarding optical and transport properties. As one can see in figure 1, the shortest intermolecular distances are in

the *b* direction and along the diagonal, in the *ab* direction. These will also be the directions where the intermolecular 'bonding' and the major interaction takes place. Consequently, the electronic properties along these directions will be influenced most strongly by pressure-induced shortening of the intermolecular atom–atom distances. It has been shown that, in an independent particle band structure of these materials, the band dispersion in these two directions and thus the total bandwidth will increase for both the valence and conduction bands [44, 46]. As a result the bandgap will decrease and the optical absorption edge will shift towards longer wavelengths upon applying hydrostatic pressure. The fluorescence quantum yield will, on the one hand, be quenched by the increased intermolecular interaction (solid state quenching) [10]. On the other hand, the increase of χ leads to an increased linear slip s (see figure 2) between the molecules and thus brings the transition dipoles further out of coparallel alignment, which will increase the respective oscillator strength [47]. The latter effect should be rather small since χ increases by only a few degrees up to the maximum pressure (see table 3). Increased band dispersion, and thus total bandwidth, will enhance the conductivity within the layers [9]. However, recent quantum chemical calculations showed that even small changes in the arrangement of molecules with respect to each other ($\Delta\chi > 0 \rightarrow \Delta s > 0$) can drastically affect the overlap between the frontier molecular one-particle wavefunctions [48]. Thus, upon applying hydrostatic pressure, one would suspect an overall, but not necessarily monotonic, increase of the conductivity.

4. Synopsis

We investigated intermolecular interactions and molecular packing in small, π-conjugated organic molecules. By performing energy dispersive x-ray powder diffraction under high hydrostatic pressure (up to 60 kbar) we probed the packing forces in polycrystalline samples of oligo(*para*-phenylenes) containing two (biphenyl) to six (*p*-sexiphenyl) phenyl rings. We found that the respective bulk moduli increase linearly with the inverse number of phenyl rings and are thus in a linear relationship with the corresponding density at ambient conditions. For the first time we report the bulk moduli B_0 and their respective pressure derivative B_0' of *p*-quaterphenyl ($B_0 = 83$ kbar, $B_0' = 6.4$), *p*-quinquephenyl ($B_0 = 93$ kbar, $B_0' = 7.5$) and *p*-sexiphenyl ($B_0 = 100$ kbar, $B_0' = 5.6$). Upon increasing hydrostatic pressure the lattice constant a decreases about twice as much as lattice constant b (and c) in all investigated materials. This causes the molecular planes to tilt more towards a cofacial alignment within one layer's herringbone pattern. The decreasing unit cell height causes the rigid rod-like molecules to give way by tilting their long axes away from being perpendicular to the *ab* plane. From these pressure-induced modifications on the molecular packing, we expect the bandgap and the optical absorption edge to shift towards lower energies, the luminescence quantum yield to decrease and the intralayer conductivity to increase.

Acknowledgments

We would like to thank Manfred Kriechbaum for help with the beamline instrumentation and the x-ray measurements and Sabine Mayer for synthesis and purification of *p*-quinquephenyl. We acknowledge the financial support of project P14237-PHY of the Austrian Fond zur Förderung der Wissenschaftlichen Forschung, the Doktorandenstipendium of the Austrian Academy of Science, the DESY-FSB project I-00-005EC and the Austrian Spezialforschungsbereich Elektroaktive Stoffe.

References

[1] Tang C W and VanSlyke S A 1987 *Appl. Phys. Lett.* **51** 913
[2] Era M, Tsutsui T and Saito S 1996 *Appl. Phys. Lett.* **67** 2436
Tasch S, Brandstätter C, Meghdadi F, Leising G, Froyer G and Athouel L 1997 *Adv. Mater.* **9** 33
[3] Dimitrakopoulos C D, Brown A R and Pomp A 1996 *J. Appl. Phys.* **80** 2501
Gundlach D J, Lin Y-Y, Jackson T N and Schlom D G 1997 *Appl. Phys. Lett.* **71** 3853
Schoonveld W A, Wildeman J, Fichou D, Bobbert P A, van Wees B J and Klapwijk T M 2000 *Nature* **404** 977
[4] Yokoyama T, Yokoyama S, Kamikado T, Okuno Y and Mashiko S 2001 *Nature* **413** 619
Kato T 2002 *Science* **295** 2414
[5] Percec V, Ahn C H, Ungar G, Yeardley D J P, Möller M and Sheiko S S 1998 *Nature* **391** 161
Sirringhaus H, Brown P J, Friend R H, Nielsen M M, Bechgaard K, Langeveld-Voss B M W, Spiering A J H, Janssen R A J, Meijer E W, Herwig P and de Leeuw D M 1999 *Nature* **401** 685
Förster S and Antonietti M 1998 *Adv. Mater.* **10** 195
[6] Zojer E, Knupfer M, Resel R, Meghdadi F, Leising G and Fink J 1997 *Phys. Rev.* B **56** 10138
Cornil J, Beljonne D, dos Santos D A, Shuai Z and Bredas J L 1996 *Synth. Met.* **78** 209
[7] Cornil J, Beljonne D, Heller C M, Campbell I H, Laurich B K, Smith D L, Bradley D D C, Müllen K and Bredas J L 1997 *Chem. Phys. Lett.* **278** 139
[8] Zojer E, Cornil J, Leising G and Bredas J L 1999 *Phys. Rev.* B **59** 7957
Cornil J, Beljonne D, Shuai Z, Hagler T W, Campbell I, Bradley D D C, Bredas J L, Spangler C W and Müllen K 1995 *Chem. Phys. Lett.* **247** 425
Kato T, Yoshizawa K and Hirao K 2002 *J. Chem. Phys.* **116** 3420
[9] Palenberg M A, Silbey R J, Malagoli M and Bredas J L 2000 *J. Chem. Phys.* **112** 1541
Cornil J, Calbert J P, Beljonne D, Silbey R and Bredas J L 2000 *Adv. Mater.* **12** 978
[10] Cornil J, Calbert J P, Beljonne D, Silbey R and Bredas J L 2001 *Synth. Met.* **119** 1
Beljonne D, Cornil J, Sirringhaus H, Brown P J, Shkunov M, Friend R H and Bredas J L 2001 *Adv. Funct. Mater.* **11** 229
[11] Yanagi H and Okamoto S 1997 *Appl. Phys. Lett.* **71** 2563
Andreev A, Matt G, Brabec C J, Sitter H, Badt D, Seyringer H and Sariciftci N S 2000 *Adv. Mater.* **12** 629
Zojer E, Koch N, Puschnig P, Meghdadi F, Niko A, Resel R, Ambrosch-Draxl C, Knupfer M, Fink J, Bredas J L and Leising G 2000 *Phys. Rev.* B **61** 16538
[12] Corney A, Manners J and Webb C E 1979 *Opt. Commun.* **31** 354
Zuev V S, Logunov O A, Savinov Y V, Startsev A V and Stoilov Y Y 1978 *Appl. Phys.* **17** 321
[13] Nogues J L, Majewski S, Walker J K, Bowen M, Wojcik R and Moreshead W V 1988 *J. Am. Ceram. Soc.* **71** 1159
[14] Tousey R and Limansky I 1972 *Appl. Opt.* **11** 1025
[15] Grem G, Leditzky G, Ulrich B and Leising G 1992 *Adv. Mater.* **4** 36
[16] Scherf U and List E J W 2002 *Adv. Mater.* **14** 477
List E J W, Holzer L, Tasch S, Leising G, Scherf U, Müllen K, Catellani M and Luzzati S 1999 *Solid State Commun.* **109** 455
[17] Thiery M M and Leger J M 1988 *J. Chem. Phys.* **89** 4255
[18] Orgzall I, Mikat J, Lorenz B, Dietel R, Knochenhauer G and Schulz B 1997 *Polymer* **38** 1537
[19] Petelenz P 1989 *Chem. Phys.* **138** 35
Matsui A, Ohno T, Mizuno K, Yokoyama T and Kobayashi M 1987 *Chem. Phys.* **111** 121
Kobayashi M, Mizuno K and Matsui A 1989 *J. Phys. Soc. Japan* **58** 809
[20] Tanaka H, Adachi T, Ojima E, Fujiwara H, Kato K, Kobayashi H, Kobayashi A and Cassoux P 1999 *J. Am. Chem. Soc.* **121** 11243
[21] Lemée-Cailleau M H, Girard A, Cailleau H, Délugeard Y and Pruzan P 1990 *Ferroelectrics* **105** 147
Girard A, Sanquer M and Délugeard Y 1985 *Chem. Phys.* **96** 427
Girard A, Cailleau H, Marqueton Y and Ecolivet C 1978 *Chem. Phys. Lett.* **54** 479
[22] Barrett R M and Steele D 1972 *J. Mol. Struct.* **11** 105
Bree A, Pang C Y and Rabeneck L 1971 *Spectrochim. Acta* A **27** 1293
Bolton B A and Prasad P N 1978 *Chem. Phys.* **35** 331
[23] Otto J W 1997 *Nucl. Instrum. Meth. Phys. Res.* A **384** 552
[24] Miyaura N, Yanagi T and Suzuki A 1981 *Synth. Commun.* **11** 513
Rehahn M, Schlüter A D, Wegner G and Feast W J 1989 *Polymer* **30** 1060
Remmers M, Schulze M and Wegner G 1996 *Macromol. Rapid Commun.* **17** 239
Scherf U and Müllen K 1991 *Macromol. Chem. Rapid Commun.* **12** 489
Inbasekaran M, Wu W W and Wu E P 1998 *US Patent Specification* No 5,777,070

[25] Jayaraman A 1983 *Rev. Mod. Phys.* **55** 65
[26] Mao H K, Xu J and Bell P M 1986 *J. Geophys. Res.* **91 (B5)** 4673
[27] Decker D L 1971 *J. Appl. Phys.* **42** 3239
[28] LeBail A and Louer D 1976 *Bull. Soc. Fr. Mineral. Cryst.* **99** 211
[29] Desiraju G R and Gavezzotti A 1989 *Acta Crystallogr.* B **45** 473
[30] Trotter J 1961 *Acta Crystallogr.* **14** 1135
[31] Charbonneau G P and Delugeard Y 1977 *Acta Crystallogr.* B **33** 1586
Hargreaves A and Hason Rizvi S 1962 *Acta Crystallogr.* **15** 365
[32] Rietveld H M, Maslen E N and Clews C J B 1970 *Acta Crystallogr.* B **26** 693
[33] Picket L W 1933 *Phil. Trans. R. Soc.* A **142** 333
[34] Delugeard Y, Desuche J and Baudour J L 1976 *Acta Crystallogr.* B **32** 702
[35] Baker K N, Fratini A V, Resch T, Knachel H C, Adams W W, Socci E P and Farmer B L 1993 *Polymer* **34** 1571
[36] Bhadra T C 1975 *Indian J. Phys.* **49** 746
[37] Birch F 1947 *Phys. Rev.* **71** 809
Birch F 1978 *J. Geophys. Res.* **83** 1257
[38] Murnaghan F D 1937 *Am. J. Math.* **59** 235
Murnaghan F D 1944 *Proc. Natl Acad. Sci. USA* **30** 244
[39] Vinet P, Ferrante J, Smith J R and Rose J H 1986 *J. Phys. C: Solid State Phys.* **19** L467
Vinet P, Smith J R, Ferrante J and Rose J H 1987 *Phys. Rev.* B **35** 1945
Vinet P, Rose J H, Ferrante J and Smith J R 1989 *J. Phys.: Condens. Matter* **1** 1941
[40] Landolt-Boernstein 1957 *Zahlenwerte und Funktionen aus Physik, Chemie, Astronomie, Geophysik und Technik* vol 2 (Berlin: Springer)
[41] Vaidya S N and Kennedy G C 1971 *J. Chem. Phys.* **55** 987
[42] Bridgman P W 1949 *Proc. Am. Acad. Sci.* **76** 9
Bridgman P W 1948 *Proc. Am. Acad. Sci.* **76** 71
Bridgman P W 1949 *Proc. Am. Acad. Sci.* **77** 129
[43] Puschnig P, Ambrosch Draxl C, Heimel G, Zojer E, Resel R, Leising G, Kriechbaum M and Graupner W 2001 *Synth. Met.* **116** 327
[44] Puschnig P, Heimel G, Weinmeier K, Resel R and Ambrosch-Draxl C 2002 *High Pressure Res.* **22** 105
[45] Oehzelt M, Weinmeier K, Heimel G, Puschnig P, Resel R, Ambrosch-Draxl C, Porsch F and Nakayama A 2002 *High Pressure Res.* **22** 343
Heimel G, Puschnig P, Weinmeier K, Zojer E, Ambrosch-Draxl C and Resel R 2001 *Mater. Res. Soc. Symp. Proc.* **665** C5.8.1
[46] Weinmeier K, Puschnig P, Ambrosch-Draxl C, Heimel G, Zojer E and Resel R 2001 *Mater. Res. Soc. Symp. Proc.* **665** C8.20.1
[47] Cornil J, Beljonne D, dos Santos D A, Calbert J P and Bredas J L 2000 *Thin Solid Films* **363** 72
[48] Cornil J, Lemaur V, Calbert J P and Bredas J L 2002 *Adv. Mater.* **14** 726
Bredas J L, Calbert J P, da Silva Filho D A and Cornil J 2002 *Proc. Natl Acad. Sci. USA* **99** 5804